Effects of Starch Nanocrystal-*graft*-Polycaprolactone on Mechanical Properties of Waterborne Polyurethane-Based Nanocomposites

Peter R. Chang,[1,2] Fujin Ai,[3] Yun Chen,[1] Alain Dufresne,[4] Jin Huang[3,4]

[1]*Bioproducts and Bioprocesses National Science Program, Agriculture and Agri-Food Canada, 107 Science Place, Saskatoon, SK, S7N 0X2, Canada*
[2]*Department of Agricultural and Bioresource Engineering, University of Saskatchewan, Saskatoon, SK, S7N 5A9, Canada*
[3]*Joint Laboratory of Polymer Modification and Functional Materials, College of Chemical Engineering, Wuhan University of Technology, Wuhan 430070, China*
[4]*École Française de Papeterie et des Industries Graphiques, Institut National Polytechnique de Grenoble (EFPG-INPG) BP65, 38402 Saint-Martin d'Hères Cedex, France*

Received 17 May 2008; accepted 27 July 2008
DOI 10.1002/app.29060
Published online 10 October 2008 in Wiley InterScience (www.interscience.wiley.com).

ABSTRACT: Based on a "graft from" strategy, the surface of starch nanocrystals (StN) were functionalized by grafting with polycaprolactone (PCL) chains via microwave assisted ring-opening polymerization (ROP). The modified natural nanoparticles were then compounded into a PCL-based waterborne polyurethane as matrix. The structural and mechanical properties of the WPU/StN-*g*-PCL nanocomposites were characterized by XRD, FTIR, SEM, DSC, DMA, and tensile testing. It was interesting to note that a loading-level of 5 wt % StN-*g*-PCL resulted in a simultaneous enhancement of tensile strength and elongation at break, both of which were higher than those of neat WPU. This enhancement was attributed to the uniform dispersion of StN-*g*-PCL because of its nano-scale size, the increased entanglements mediated with grafted PCL chains, and the reinforcing function of rigid StN. Increasing the StN-*g*-PCL content however caused the StN-*g*-PCL to self-aggregate as crystalline domains, which impeded improvement in tensile strength and elongation at break, but significantly enhanced Young's modulus. © 2008 Wiley Periodicals, Inc. J Appl Polym Sci 111: 619–627, 2009

Key words: waterborne polyurethane; starch nanocrystals; graft; nanocomposite; mechanical properties; structure-properties relationship

INTRODUCTION

Renewable biopolymers have found unique applications as matrices, nano-fillers, or both in new "green" bionanocomposites.[1–3] Emerging nano-fillers, derived from natural polysaccharides, are those in crystalline form with uniform structure and high rigidity and act as the ingredients of choice for bionanocomposites. Besides exhibiting a reinforcing function similar to inorganic nano-fillers,[4–8] natural nano-fillers are readily availability and nontoxic and also contribute biodegradability, biocompatibility, high reactivity, and easy processability owing to their nonabrasive nature.[4] In contrast to the rod-like whiskers of cellulose[4] and chitin,[5] starch nanocrystals show a distinct platelet-like structure[9,10] similar to that of exfoliated layered silicate.[11,12] However, starch nanocrystals self-aggregate easily and form agglomerates in micrometer scale, inhibiting their function in composites. Fortunately, starch nanocrystals have reactive surfaces suitable for chemical derivation and grafting reactions.[13–16] Such modification would facilitate the dispersion of starch nanocrystals, manipulate the hydrophobicity of surface, and improve the miscibility between the starch nanocrystals and the polymer matrix. Particularly, grafting produces long tails on the surface of starch nanocrystals which may penetrate into the polymer matrix and exert a stronger interfacial interaction.

Correspondence to: P. R. Chang (changp@agr.gc.ca) and J. Huang (huangjin@iccas.ac.cn).

Contract grant sponsor: Agricultural Bioproducts Innovation Program (ABIP) of Canada via the Pulse Research Network (PURENET).
Contract grant sponsor: Youth Chenguang Program of Science & Technology in Wuhan; contract grant number: 200850731383.
Contract grant sponsor: State Key Laboratory of Polymer Physics and Chemistry (Changchun Institute of Applied Chemistry, Chinese Academy of Sciences).
Contract grant sponsor: Key Laboratory of Cellulose and Lignocellulosics Chemistry, Guangzhou Institute of Chemistry, Chinese Academy of Sciences; contract grant numbers: LCLC-2005-172 and LCLC-2008-02.

Because of the increasing concern for human health and environmental-friendliness, materials science has developed an organic solvent-free polyurethane (i.e., waterborne polyurethane) which is nontoxic and has low volatile organic compounds (VOC).[17,18] To enhance the strength and modulus of waterborne polyurethane-based elastomers, there have been attempts to fill the waterborne polyurethane matrix with inorganic nanoparticles.[19–21] Meanwhile, natural polymers[22–26] have been compounded into waterborne polyurethane matrices by mechanical blending or interpenetrating polymer networks to improve biodegradability. Recently, rod-like cellulose whiskers and platelet-like starch nanocrystals have also been incorporated into waterborne polyurethane matrices, resulting in a significant improvement in mechanical performance.[27,28]

In this work, the surface of starch nanocrystals (StN) was functionalized by grafting polycaprolactone (PCL) chains based on the "graft from" strategy from our previous work.[29] The soft-segment, with the same origin as grafted PCL chains, was therefore selected as the component of waterborne polyurethane matrix. Compared with the previous report on the Poly(1,4-butylene glycol adipate)-based waterborne polyurethane modified by neat StN,[28] the same structure for soft-segment and grafted chains on the surface of StN could improve the association between waterborne polyurethane as matrix and the StN-*g*-PCL nano-filler. Furthermore, the simultaneous reinforcing and toughening of waterborne polyurethane, attributed to the introducing of rigid platelet-like StN, is expected, in contrast with the contribution of rod-like cellulose whisker to the increase of only strength and modulus of PCL-based waterborne polyurethane.[27] The structural and mechanical properties of the resultant nanocomposite materials were subsequently investigated by Fourier transform infrared spectroscopy (FTIR), X-ray diffraction (XRD), differential scanning calorimetry (DSC), dynamic mechanical analysis (DMA), scanning electron microscope (SEM), and tensile testing. Furthermore, the effects of StN-*g*-PCL on mechanical properties of waterborne polyurethane-based nanocomposites were explored while the key role of grafted PCL chains in enhancing mechanical properties was realized by structural analysis.

EXPERIMENTAL

Materials

Polycaprolactone diol with number-average molar weight (M_n) of 2000 (PCL_{2000}) was purchased from Sigma-Aldrich, and dried under vacuum for 12 h before use. Dimethylol propionic acid (DMPA) was donated by Huzhou Changsheng Co. Ltd. (Zhejiang, China), and dried under vacuum at 80°C for 12 h before use. Toluene diisocyanate (TDI) and triethylamine (TEA) were purchased from Sinopharm Chemical Reagent Co. Ltd. (Shanghai, China), and redistilled before use. Pea starch composed of 35% amylose and 65% amylopectin, and with average particle size of about 30 μm, was supplied by Nutri-Pea Limited Canada (Portage la Prairie, Canada) and used as received. The ε-caprolactone (CL) monomer was purchased from Alfa Aesar, and used as received. Tin(II) octoate ($Sn(Oct)_2$), sulfuric acid (H_2SO_4) and other reagents of analytical grade were purchased from the Shanghai Sinopharm Chemical Co. Ltd (Shanghai, China), and used as received.

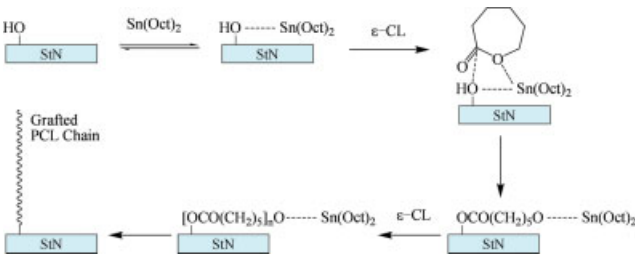

Scheme 1 Schematical illustration of grafting PCL chains onto the StN surface via microwave assisted ring-opening polymerization.

Extraction and grafting of starch nanocrystals

The starch nanocrystals (StNs) were prepared, as previously reported,[30] by H_2SO_4 hydrolysis of native pea starch granules. Pea starch granules (14.69 g) were dispersed in 100 mL of 3.16*M* H_2SO_4, and stirred at 100 rpm for 5 days at 40°C. The resultant suspension was washed by successive centrifugation with distilled water until approximate neutrality. Subsequently, a small amount of ammonia was added followed by dialysis overnight with distilled water. The StN powder was then obtained by lyophilization.

Ring-opening polymerization (ROP) under microwave irradiation was used to prepare StN-*g*-polycaprolactone (StN-*g*-PCL) (seen in Scheme 1). The StN powder and ε-caprolactone (CL) monomer, a weight ratio of StN versus CL of 1:10, were placed into an ampoule. The $Sn(Oct)_2$ catalyst was added at a rate of 5%, based on the CL weight. The mixture was homogenized by a Lab Dancer compact shaker (IKA), and then vacuum-degassed for 30 min. The ampoule containing the reactant was conditioned under microwave irradiation of 255-W power for 5 min. Finally, the crude product was dissolved in dichloromethane followed by precipitating with methanol. This process of purification was carried out three times to remove the monomer and the residual catalyst. The purified product was vacuum-dried, and

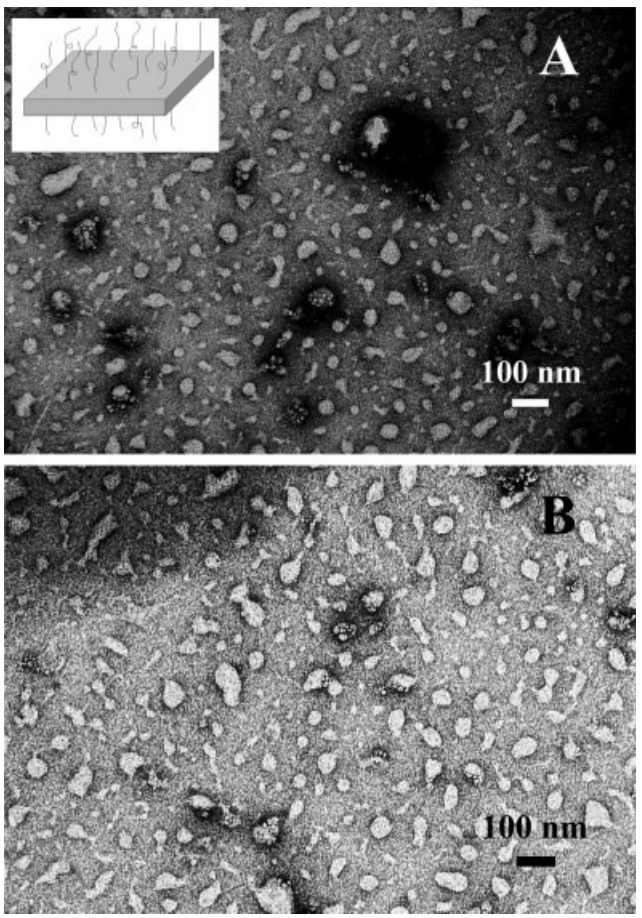

Figure 1 Schematic illustration and TEM image of StN-*g*-PCL nanoparticles (A) and their dispersion states in the polyurethane solution (B).

coded as StN-*g*-PCL. In our previous report,[29] the grafted PCL content in StN-*g*-PCL was determined, by element analysis, to be 84.16 wt %. TEM images showed most of the StN-*g*-PCL nanoparticles were platelet-like in structure and less than 100 nm (Fig. 1A).

Preparation of WPU-based nanocomposite filled with StN-*g*-PCL

To prepare the StN-*g*-PCL modified waterborne polyurethane (WPU) films, PCL_{2000} and TDI were placed into a three-necked round-bottom flask equipped with a mechanical stirrer and a reflux condenser. The flask was heated to $\sim$ 65°C, and stirred for 2 h under dry nitrogen. DMPA, a chain-extender, was dispersed in acetone and added to the flask to give a NCO/OH molar ratio of 1.8. The temperature was elevated to 75°C for another hour. During this period, acetone was occasionally added to lower the viscosity of the reactant. The resulting product was cooled to below 40°C before TEA was added to neutralize the —COOH of DMPA in the polyurethane chains. Subsequently, the designated amount StN-*g*-PCL was dispersed in acetone and added to the mixture under severe mechanical stirring to produce a blend. The dispersion states of StN-*g*-PCLs in the blend solution were depicted in Figure 1B, which is almost same as the TEM observation of Figure 1A. Ice water was then added to form an emulsion with a solids content of 20 wt %. The WPU emulsion containing StN-*g*-PCL was cast into a Teflon mold after vacuum degassing, and solidified as a film at 50°C by evaporation. The neat WPU was prepared using the above-mentioned process without adding StN-*g*-PCL.

The resulting films with a thickness of $\sim$ 0.5 mm were vacuum-dried overnight and kept in a desiccator with silica gel desiccant. These films were coded, according to the StN-*g*-PCL content in the blends, as WPU/StN-g-PCL(5), WPU/StN-*g*-PCL(10), WPU/StN-*g*-PCL(15), WPU/StN-*g*-PCL(20), WPU/StN-*g*-PCL(25), and WPU/StN-*g*-PCL(30), where the numbers in brackets represent the theoretical weight percentage of StN-*g*-PCL in the films. The neat WPU film without StN-*g*-PCL was coded as WPU-F.

Characterization

The Fourier transform infrared (FTIR) spectra of all the films were recoded on a FTIR 5700 spectrometer (Nicolet, USA) using Smart OMNT reflect accessories in the range of 4000–700 cm^{-1}.

X-ray diffraction (XRD) measurements were performed on a D/max-2500 X-ray diffractometer (Rigaku Denki, Japan) with Cu $K\alpha_1$ radiation (λ = 0.154 nm) in a range of $2\theta = 3 - 60°$ using a fixed time mode with a step interval of 0.02°.

Scanning electron microscope (SEM) observation was carried out on an *S*-3000*N* scanning electron microscope (Hitachi, Japan). The films were frozen in liquid nitrogen and then immediately snapped. The fracture surfaces of the films were sputtered with gold, and then observed and photographed.

Transmission electron microscope (TEM) observation was carried out on an H-7000FA electron microscope (Hitachi, Japan) at 75 kV. A small amount of StN-*g*-PCL was dissolved in dichloromethane, and then dispersed in distilled water followed by rotating evaporation to remove dichloromethane. Furthermore, the mixing solution containing StN-*g*-PCL and polyurethane in acetone was dispersed in distilled water followed by rotating evaporation to remove acetone. Two StN-*g*-PCL suspensions were respectively, diluted as a concentration of $\sim$ 0.5 wt %, and then negatively stained with 2% (w/v) aqueous solution of uranyl acetate.

Differential scanning calorimetry (DSC) analysis was carried out on a DSC-Q200 instrument (TA Instruments, USA) under a nitrogen atmosphere at a heating or cooling rate of 20°C min^{-1}. The films

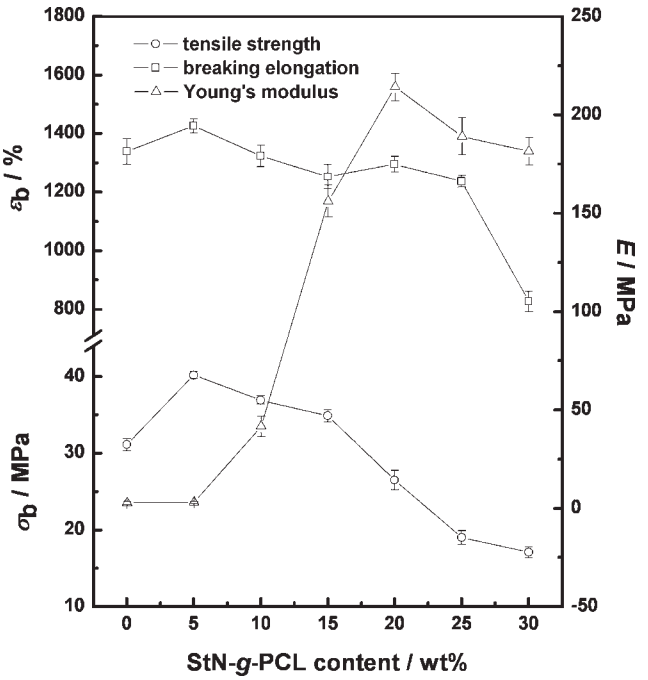

Figure 2 Effects of StN-*g*-PCL content on tensile strength (σ_b), elongation at break (ε_b), and Young's modulus (E) for WPU/StN-*g*-PCL nanocomposite films and neat WPU-F film reference.

were scanned in the range of −90 to 200°C after a pretreatment (heating from 20 to 100°C and then cooling down to −90°C) to eliminate thermal history.

Dynamic mechanical analysis (DMA) was carried out on a DMA 242C dynamic mechanical analyzer (Netzsch, Germany) using a dual cantilever device at a frequency of 1 Hz. The temperature ranged from −150 to 100°C with a heating rate of 2°C min^{-1}. The dimensions of the testing specimens, with a thickness of ~ 0.5 mm, were 30 mm × 10 mm.

The tensile strength (σ_b), elongation at break (ε_b), and Young's modulus (E) of all the films were measured on a CMT6503 universal testing machine (SANS, Shenzhen, China) with a tensile rate of 100 mm min^{-1} according to ISO527-3:1995(E). The films were cut as quadrate strips with a width of 10 mm. The distance between testing marks was 40 mm. The tested strips were kept in relative humidity of 35% for 7 days before measurement. Five replicates were performed on each film and the average value was calculated.

RESULTS AND DISCUSSION

Mechanical properties of WPU/StN-*g*-PCL nanocomposites

The effects of StN-*g*-PCL content on the mechanical properties, including tensile strength (σ_b), Young's modulus (E), and elongation at break (ε_b), of WPU-based nanocomposite films are depicted in Figure 2. In contrast to a tensile strength of 31.12 MPa for the neat WPU-F film, the WPU/StN-*g*-PCL(5), containing 5 wt % StN-*g*-PCL, showed a maximum tensile strength of 40.19 MPa. As the StN-*g*-PCL content increased, the tensile strength gradually decreased to even lower than that of neat WPU-F when the StN-*g*-PCL content was greater than 20 wt %. It is worth noting that the elongation of WPU/StN-*g*-PCL(5) was enhanced (namely a simultaneous reinforcing and toughening). However, with an increase in StN-*g*-PCL content, the elongation decreased and was lower than that of WPU-F. Except for the Young's modulus for WPU/StN-*g*-PCL(5), which was close to that of WPU-F, the Young's modulus values of nanocomposites with higher StN-*g*-PCL content increased significantly. This indicated that the addition of StN-*g*-PCL enhanced the rigidity of the nanocomposite materials. When the StN-*g*-PCL content was higher than 20 wt % however, the Young's modulus showed a slight decreasing tendency.

Structures of WPU/StN-*g*-PCL nanocomposites

XRD patterns for the WPU/StN-*g*-PCL nanocomposite films as well as for neat WPU-F, PCL_{2000}, and StN-*g*-PCL are shown in Figure 3. The PCL_{2000}

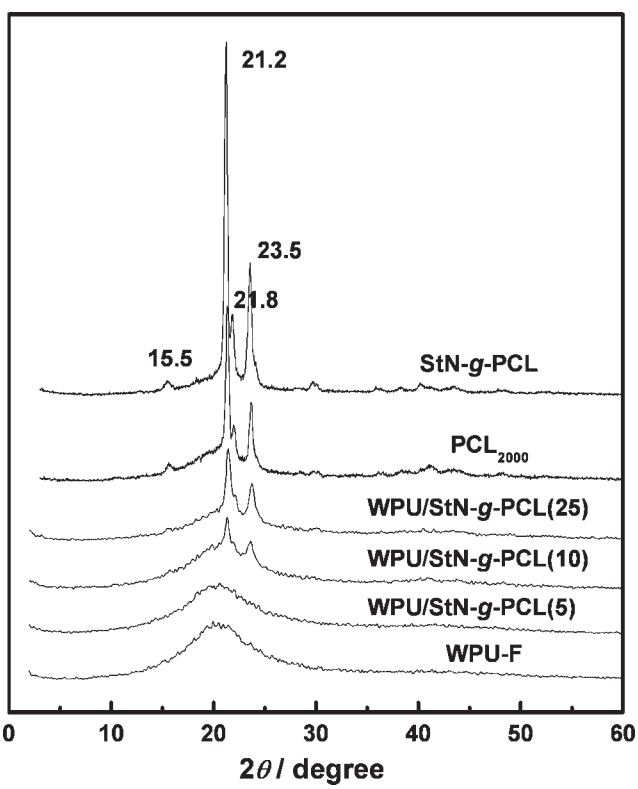

Figure 3 XRD patterns of WPU/StN-*g*-PCL nanocomposite films containing various loading-levels of StN-*g*-PCL and StN-*g*-PCL, WPU-F, and PCL_{2000} as references.

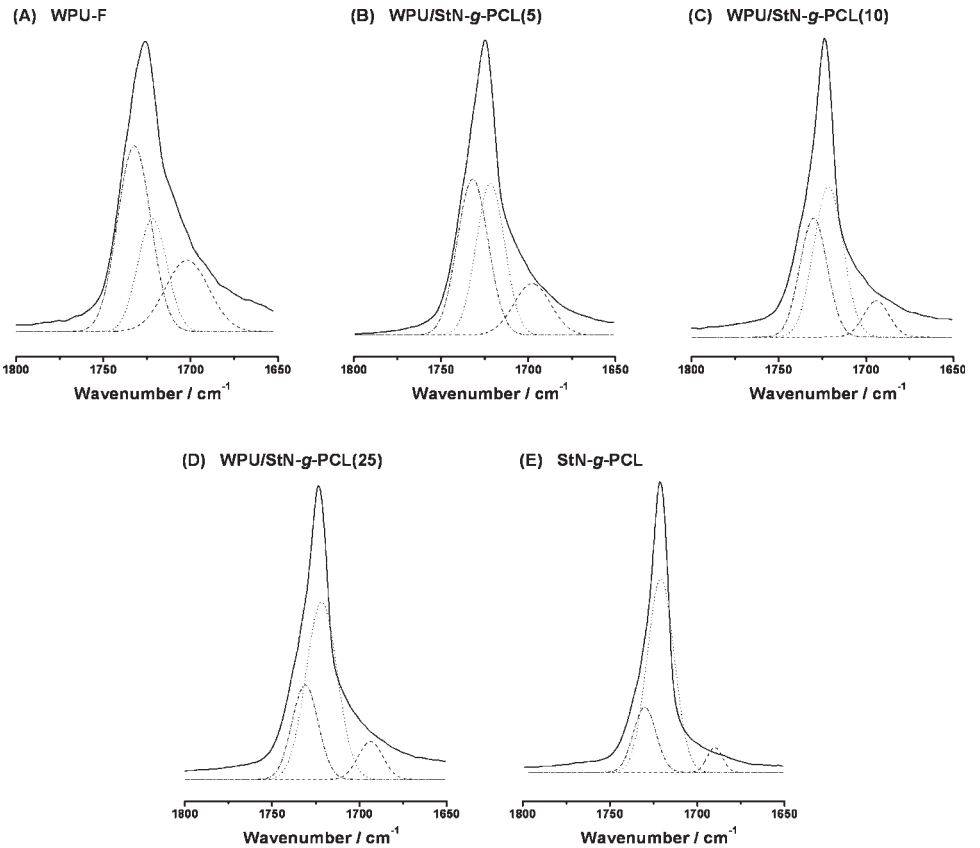

Figure 4 Experimental and curve-fitted FTIR spectra of WPU/StN-*g*-PCL nanocomposite films and neat WPU-F and StN-*g*-PCL in the range of 1600–1800 cm^{-1}. (—— experimental curve; -·-·- —C=O in amorphous region; ····· —C=O in crystalline domain; ---- hydrogen-bonded —C=O).

showed two strong diffraction peaks located at 21.2° and 23.5° of 2θ as well as two weak diffraction peaks at 15.5° and 21.8° of 2θ. The grafted PCL chains onto StN-*g*-PCL showed crystalline diffraction similar to PCL_{2000}, but the diffraction intensities were obviously stronger. However, neat WPU-F showed a diffuse diffraction with the peak located at around 20.5° of 2θ, indicating that PCL_{2000}, as the soft-segment of WPU, was mainly in an amorphous state. At the lowest loading-level of StN-*g*-PCL (i.e., 5 wt %), the diffraction pattern of WPU/StN-*g*-PCL(5) was similar to that of WPU-F. This may be attributed to the homogeneous dissolution of StN-*g*-PCL in the WPU matrix. When the StN-*g*-PCL content was increased to 10 wt %, the character diffraction peaks assigned to the PCL component were visible. As the StN-*g*-PCL content increased, the intensities of diffraction peaks increased as well, which may be attributed to self-aggregation of StN-*g*-PCL as greater crystalline domain.

Experimental and curve-fitted FTIR spectra of the WPU/StN-*g*-PCL nanocomposite films as well as the neat WPU-F and StN-*g*-PCL in the range of 1600–1800 cm^{-1} are shown in Figure 4. The location and fraction of Curve-Fitting Peaks for —C=O absorption are summarized in Table I, including Peak I located at ~ 1731 cm^{-1} and Peak II located at 1721 cm^{-1} for —C=O in the amorphous region and the crystalline domain respectively, as well as Peak III located the lowest wavenumber for hydrogen-bonded —C=O. Since the content of —C=O assigned to PCL_{2000} as soft-segments and the grafted PCL chains onto StN-*g*-PCL were much higher than —C=O in hard-segments, the contribution of —C=O in hard-segments to the —C=O absorption in FTIR spectra might be neglected. The fraction of hydrogen-bonded —C=O absorption (Peak III) in StN-*g*-PCL was lowest at 5.48% while the fractions of Peak III for the WPU/StN-*g*-PCL nanocomposites were lower than that of neat WPU-F. This suggests that hydrogen bonding in the WPU matrix was partly destroyed after introducing StN-*g*-PCL. At the same time, with an increase in StN-*g*-PCL content, the fraction of —C=O absorption in the crystalline domain (Peak II) increased while that of —C=O absorption in the amorphous region (Peak I) decreased. This is consistent with the XRD results, namely, the diffraction assigned to the PCL component occurred when the StN-*g*-PCL content was higher.

TABLE I
Location and Fraction of Curve-Fitting Peaks for the —C=O absorption in FTIR Spectra of the WPU/StN-*g*-PCL Nanocomposites with various StN-*g*-PCL content, neat WPU-F, and StN-*g*-PCL

	—C=O assigned to PCL component					
	Peak I		Peak II		Peak III	
Sample code	Location/cm^{-1}	Fraction/%	Location/cm^{-1}	Fraction/%	Location/cm^{-1}	Fraction/%
WPU-F	1732.2	49.06	1721.8	26.08	1701.9	24.86
WPU/StN-*g*-PCL (5)	1731.8	43.50	1721.6	39.19	1697.7	17.32
WPU/StN-*g*-PCL (10)	1729.9	37.68	1721.4	51.51	1694.0	10.81
WPU/StN-*g*-PCL (25)	1731.1	27.66	1721.6	61.72	1693.6	10.62
StN-g-PCL	1730.0	20.88	1720.9	73.64	1689.9	5.48

Peak I: —C=O in Amorphous Region; Peak II: —C=O in Crystalline Domain; Peak III: hydrogen-bonded —C=O.

Fractured surfaces of WPU/StN-*g*-PCL nanocomposites

Figure 5 shows the SEM images of fracture surfaces of the WPU/StN-*g*-PCL nanocomposite films and WPU-F. The WPU-F without StN-*g*-PCL showed a fluctuant fracture surface with many pleats. The fracture surface of WPU/StN-*g*-PCL(5), with the lowest loading level, was similar to that of WPU-F, but the pleats were smaller. This indicated that there were more entanglements in WPU/StN-*g*-PCL(5) than those in WPU-F, which facilitated the increase of elongation. When the StN-*g*-PCL content was higher (such as WPU/StN-*g*-PCL(10) and WPU/StN-*g*-PCL(25)), the faultage-like structure occurred on the fractured surface. Furthermore, with an increase in the StN-*g*-PCL content, the density of faultages increased. This may be attributed to the forming of crystalline domains based on self-aggregated StN-*g*-PCL. This brittle-fracture nature is consistent with the decrease in strength and elongation as well as the increase in Young's modulus for the WPU/StN-*g*-PCL with higher loading-levels of StN-*g*-PCL.

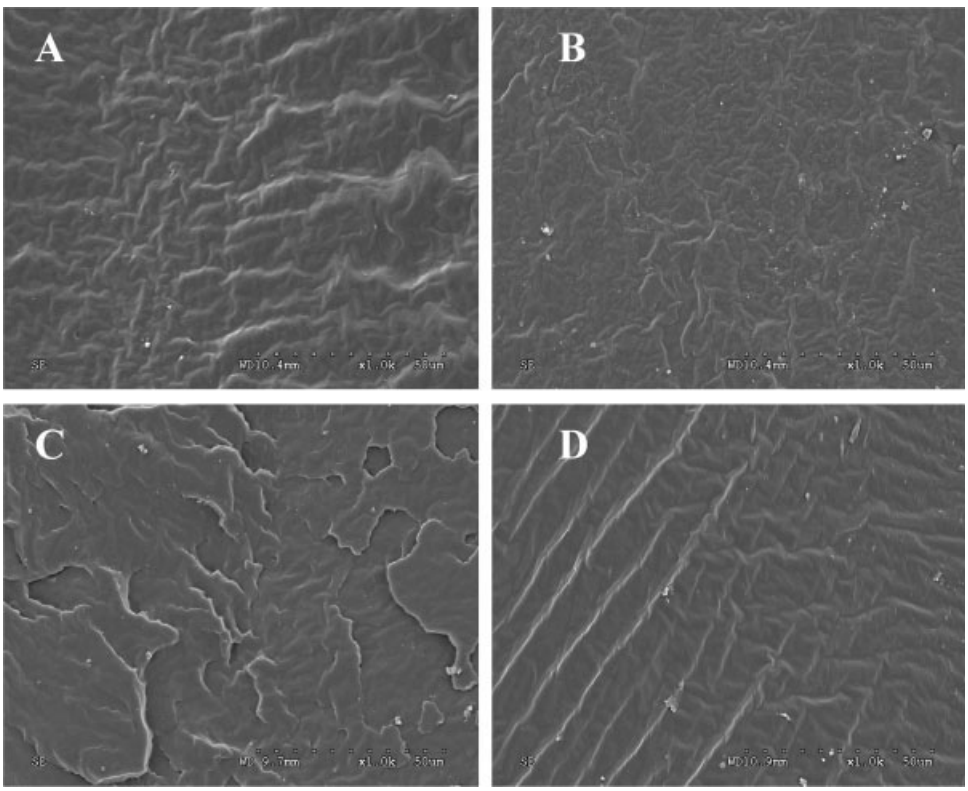

Figure 5 SEM images of fracture surfaces of WPU/StN-*g*-PCL nanocomposite films containing various loading-levels of StN-*g*-PCL and WPU-F reference. (A: WPU-F; B: WPU/StN-*g*-PCL(5); C: WPU/StN-*g*-PCL(10); D: WPU/StN-*g*-PCL(25)).

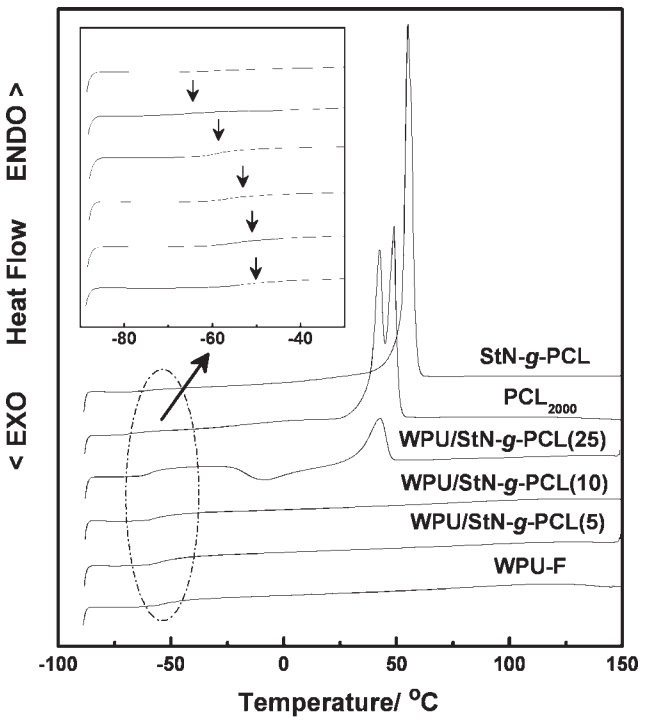

Figure 6 DSC thermograms of WPU/StN-*g*-PCL nanocomposite films containing various loading-evels of StN-*g*-PCL and StN-*g*-PCL, WPU-F and PCL_{2000} references.

Thermal Properties of WPU/StN-*g*-PCL nanocomposites

DSC thermograms of the WPU/StN-*g*-PCL nanocomposite films as well as thermograms for the neat WPU-F, PCL_{2000}, and StN-*g*-PCL films are depicted in Figure 6. The data for glass transition temperature at midpoint ($T_{g,\mathrm{mid}}$) and heat-capacity increment (ΔC_p) as well as melting temperature (T_m) and heat enthalpy (ΔH_m) are summarized in Table II. Besides glass transition inhibited by highly crystalline StN-*g*-PCL, all the WPU/StN-*g*-PCL nanocomposites, WPU-F and PCL_{2000} as the substance of WPU showed the process of glass transition. The $T_{g,\mathrm{mid}}$s assigned to the PCL component in WPU-F and WPU/StN-*g*-PCLs were higher than that of PCL_{2000}, owing to lower freedom of motion confined by the hard-segments in WPU and the StN-*g*-PCL nano-filler. Furthermore, the $T_{g,\mathrm{mid}}$s of WPU/StN-*g*-PCLs were lower than that of neat WPU-F. This was attributed to the cleavage of the hydrogen bonds between the soft- and hard-segments in the WPU matrix, which was consistent with the FTIR analysis. WPU-F had no melting transition of PCL in spite of the fact that the $PCL_{2000,}$ as the substance of the soft-segment, had a melting transition that appeared as one double-peak. With an increase in the StN-*g*-PCL content, the melting transition assigned to the PCL component occurred for WPU/StN-*g*-PCL(25), which verified the XRD results. However, it was still puzzling why the WPU/StN-*g*-PCL(10) with the crystalline diffraction in XRD pattern had no melting transition in many DSC tests. DMA tests also provided additional proof for the motion of soft-segment at molecular-level by observing α-relaxation, the α-relaxation temperature at onset ($T_{\alpha,\mathrm{onset}}$) and the corresponding storage modulus ($\log E'$) from $\log E' - T$ curves (Fig. 7) as well as the temperature ($T_{\alpha,\mathrm{max}}$) and height ($H_{\mathrm{loss\text{-}peak}}$) of loss-peak from $\tan\delta - T$ curves (Fig. 7) are listed in Table II. The $T_{\alpha,\mathrm{onset}}$s and $T_{\alpha,\mathrm{max}}$s of the WPU/StN-*g*-PCL nanocomposites were also lower than those of neat WPU-F, mainly owing to the unbinding of soft-segments from hard-segments in WPU matrix by cleaving hydrogen bonds. In the $\tan\delta - T$ curves, the WPU/StN-*g*-PCL(5) with lowest loading-level of StN-*g*-PCL showed an increased magnitude of loss-peak, suggesting that the energy dissipation process is quicken up by the nano-fillers. It is attributed to the cleavage of hydrogen bonds between the soft- and hard-segments in spited that the improved associations between soft-segments and grafted PCL chains might inhibit the motion of soft-segments. However, with an increase of StN-*g*-PCL loading-level, the magnitude of loss-peaks for the WPU/StN-*g*-PCL nanocomposites containing higher than 10 wt % StN-*g*-PCL reduced. It means that the interactions between the soft-segments in WPU matrix and the StN-*g*-PCL nano-fillers mediated with grafted PCL

TABLE II
DSC and DMA Data for WPU/StN-*g*-PCL Nanocomposites of Various StN-*g*-PCL Content, Neat WPU-F, StN-*g*-PCL, and PCL_{2000}

Sample	DSC Data				DMA Data			
	$T_{g,\mathrm{mid}}$/°C	ΔC_p/J g^{-1} K^{-1}	T_m/°C	ΔH_m/J g^{-1}	$T_{\alpha,\mathrm{onset}}$/°C	Log E'	$T_{\alpha,\mathrm{max}}$/°C	$H_{\mathrm{loss\text{-}peak}}$
WPU-F	−53.79	0.288	–	–	−41.76	3.27	−25.22	0.157
WPU/StN-*g*-PCL (5)	−54.95	0.310	–	–	−56.69	3.29	−38.68	0.171
WPU/StN-*g*-PCL (10)	−56.94	0.307	–	–	−51.16	3.31	−31.80	0.100
WPU/StN-*g*-PCL (25)	−59.35	0.257	42.17	30.46	−50.92	3.10	−29.52	0.092
StN-g-PCL	–	–	55.02	76.35	–	–	–	–
PCL_{2000}	−66.83	0.144	42.49/48.85	68.81	–	–	–	–

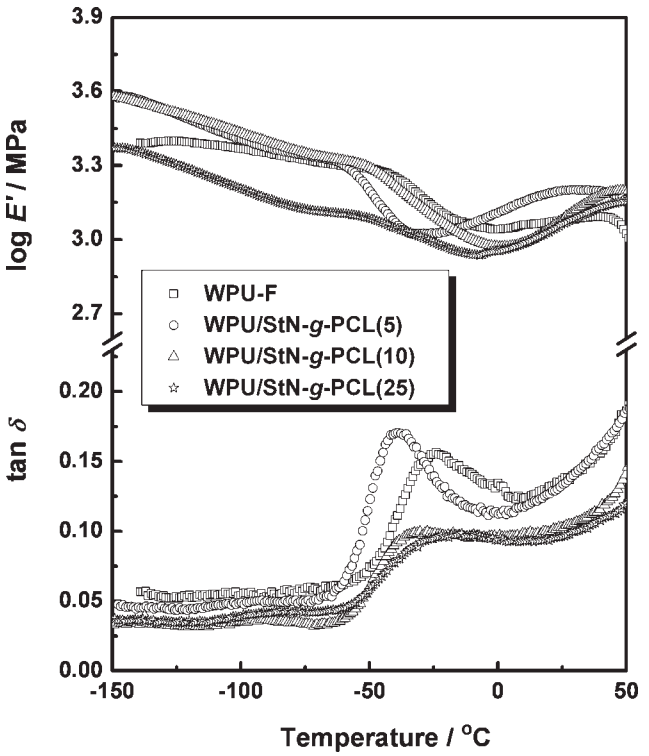

Figure 7 Storage modulus (log E') and loss factor (tanδ) as functions of temperature for WPU/StN-*g*-PCL nanocomposite films containing various loading-levels of StN-*g*-PCL and WPU-F reference.

chains, as well as the steric hindrance of the StN-*g*-PCL nano-fillers, decreased the mobility of soft-segment.[31]

Role of StN-*g*-PCL in WPU-based nanocomposites

It is well known that the mechanical properties of nanocomposites are relevant to the coroperative effects of several factors besides the structural strange of matrix, such as the nanoparticle/matrix interactions as well as the dispersing scale, morphology and surface functionality of the nanoparticles. The grafted PCL chains as the surface functionality of StN was the same origin as the PCL_{2000} as soft segment of WPU, and hence improved the miscibility between StN and the WPU matrix in nanocomposites. As a result, the reinforcing function of StN as the center of stress-concentration could be fully played, resulting in an enhancement of strength. At the same time, increasing entanglements mediated with grafted PCL chains facilitated the increase of elongation. Such improvements were based on the uniform dispersion of the StN-*g*-PCL nanoparticles. Once the StN-*g*-PCL self-aggregated as crystalline domains, the strength and elongation decreased. However, the rigidity of the StN-*g*-PCL crystalline domains contributed to the increase in Young's modulus.

CONCLUSIONS

We functionalized the surface of starch nanocrystals (StNs) by growing polycaprolactone (PCL) chains via microwave assisted ring-opening polymerization (ROP). The modified nanoparticles were then loaded into a waterborne polyurethane (WPU) matrix. The WPU/StN-*g*-PCL(5) containing the lowest load level of 5 wt % StN-*g*-PCL showed a maximum tensile strength and elongation higher than those of neat WPU. In this case, the simultaneous enhancement in strength and elongation was attributed to the uniform dispersion of the nano-scale StN-*g*-PCL as well as increasing entanglements mediated with grafted PCL chains, and the reinforcing function of rigid StN. However, with an increase in the StN-*g*-PCL content, the StN-*g*-PCL self-aggregated as crystalline domains which impeded the improvement in tensile strength and elongation at break, though Young's modulus was significantly enhanced. To our knowledge, this is the first report on modifying waterborne polyurethane based on polymer-grafted natural nanocrystal. Meanwhile, the same origin for soft-segment in waterborne polyurethane matrix and grafted polymer chains onto starch nanocrystal has been considered as a key factor to enhance mechanical properties. Moreover, high mechanical performances of such new nanocomposite material based on biodegradable compositions could be believed to have great potential applications.

References

1. Darder, M.; Aranda, P.; Ruiz-Hitzky, E. Adv Mater 2007, 19, 1309.
2. Yu, L.; Dean, K.; Li, L. Prog Polym Sci 2006, 31, 576.
3. Yang, K.-K.; Wang, X.-L.; Wang, Y.-Z. J Ind Eng Chem 2007, 13, 485.
4. Azizi Samir, M. A. S.; Alloin, F.; Dufresne, A. Biomacromolecules 2005, 6, 612.
5. Paillet, M.; Dufresne, A. Macromolecules 2001, 34, 6527.
6. Angellier, H.; Molina-Boisseau, S.; Dole, P.; Dufresne, A. Biomacromolecules 2006, 7, 531.
7. Angellier, H.; Molina-Boisseau, S.; Dufresne, A. Macromolecules 2005, 38, 9161.
8. Yuan, H.; Nishiyama, Y.; Wada, M.; Kuga, S. Biomacromolecules 2006, 7, 696.
9. Putaux, J.-L.; Molina-Boisseau, S.; Momaur, T.; Dufresne, A. Biomacromolecules 2003, 4, 1198.
10. Angellier, H.; Choisnard, L.; Molina-Boisseau, S.; Ozil, P.; Dufresne, A. Biomacromolecules 2004, 5, 1545.
11. Jiang, L.; Zhang, J.; Wolcott, M. P. Polymer 2007, 48, 7632.
12. Yu, Z.; Yin, J.; Yan, S; Xie, Y; Ma, J; Chen, X Polymer 2007, 48, 6439.
13. Angellier, H.; Molina-Boisseau, S.; Belgacem, M. N.; Dufresne, A. Langmuir 2005, 21, 2425.
14. Thielemans, W.; Belgacem, M. N.; Dufresne, A. Langmuir 2006, 22, 4904.
15. Labet, M.; Thielemans, W.; Dufresne, A. Biomacromolecules 2007, 8, 2916.
16. Song, S.; Wang, C.; Pan, Z.; Wang, X. J Appl Polym Sci 2008, 107, 418.

17. Wicks, Z. W.; Wicks, D. A.; Rosthauser, J. W. Prog Org Coat 2002, 44, 161.
18. Noble, K. L. Prog Org Coat 1997, 32, 131.
19. Chattopadhyay, D. K.; Raju, K.V. S. N. Prog Polym Sci 2007, 32, 352.
20. Kuan, H. C.; Chuang, W. P.; Ma, C. C. M. J Mater Sci 2005, 40, 179.
21. Kwon, J; Kim, H. J Polym Sci Part A Polym Sci 2005, 43, 3973.
22. Wu, Q.; Zhang, L. J Appl Polym Sci 2001, 79, 2006.
23. Lu, Y. S.; Tighzert, L.; Dole, P.; Erre, D. Polymer 2005, 46, 9863.
24. Lu, Y. S.; Tighzert, L.; Berzin, F.; Rondot, S. Carbohydr Polym 2005, 61, 174.
25. Wang, N.; Zhang, L. Polym Int 2005, 54, 233.
26. Cui, G.; Xia, W.; Chen, G.; Wei, M.; Huang, J. J Appl Polym Sci 2007, 106, 4257.
27. Cao, X.; Dong, H.; Li, C. M. Biomacromolecules 2007, 8, 899.
28. Chen, G.; Wei, M.; Chen, J.; Huang, J; Dufresne, A; Chang, P. R. Polymer 2008, 49, 1860.
29. Yu, J; Ai, F.; Dufresne, A.; Gao, S.; Huang, J.; Chang, P. R. Macromol Mater Eng 2008, 293, 763.
30. Zheng, H.; Ai, F.; Chang, P. R.; Huang, J.; Dufresne, A. Polym Compos. DOI: 10.1002/pc.20612.
31. Chausson, S.; Caignaert, V.; Retous, R.; Rueff, J.; -M.; Pluart, L L; Madec, P-J; Jaffrès, P-A Polymer 2008, 49, 488.